Available online at www.sciencedirect.com
SCIENCE DIRECT®
Applied Catalysis A: General 265 (2004) 141–152
APPLIED CATALYSIS A: GENERAL
www.elsevier.com/locate/apcata

Crystal phase dependent metal–support interactions in Pt/SO_4^{2-}-ZrO_2 catalysts for hydroconversion of *n*-alkanes

Javier M. Grau [a], Juan C. Yori [a], Carlos R. Vera [a,*], Francisco C. Lovey [b], Adriana M. Condó [c], José M. Parera [a]

[a] *Instituto de Investigaciones en Catálisis y Petroquímica, INCAPE (FIQ-UNL-CONICET), Santiago del Estero 2654, 3000 Santa Fe, Argentina*
[b] *Centro Atómico Bariloche, Comisión Nacional de Energía Atómica, 8400 San Carlos de Bariloche, Argentina*
[c] *Consejo Nacional de Investigaciones Científicas y Técnicas, 1033 Buenos Aires, Argentina*

Received in revised form 12 January 2004; accepted 14 January 2004

Available online 15 April 2004

Abstract

In order to elucidate the influence of the crystal structure of zirconia on the properties of the metallic and acid function of Pt/SO_4^{2-}-ZrO_2, catalysts with different zirconia crystal phases were synthesized, fully tetragonal, fully monoclinic, and with a mixture of the tetragonal and monoclinic phases. Their catalytic properties were studied in the metal-catalyzed reaction of cyclohexane dehydrogenation (300 °C, 0.1 MPa, WHSV = 10 h^{-1}, H_2/C_6H_{12} = 30), the acid-catalyzed isomerization of *n*-butane (350 °C, 0.1 MPa, WHSV = 1 h^{-1}, H_2/C_4H_{10} = 6), and the bifunctional hydroconversion of *n*-octane (300 °C, 1.5 MPa, WHSV = 4 h^{-1}, H_2/C_8H_{18} = 6). TPR, XRD and FTIR of chemisorbed CO were also used in order to characterize the catalysts. The results showed a strong influence of the crystal phase on the activity of the acid function. A less marked effect was found for the metal-catalyzed reaction. An opposite relation between the two functions was seen with respect to this crystal structure influence. Among the sulfated catalysts, monoclinic Pt/SO_4^{2-}-ZrO_2 had the lowest activity in *n*-C_4 isomerization and the highest activity in cyclohexane dehydrogenation. Tetragonal Pt/SO_4^{2-}-ZrO_2 catalysts were the most active in isomerization of *n*-butane. They had the lowest activity in cyclohexane dehydrogenation and their metal properties were negligible. They were also the most active in *n*-C_8 conversion, producing mainly *i*-C_4. Monoclinic catalysts had low cracking activity and produced mainly isooctane. Mixed phase catalysts had an intermediate behavior.

While S poisoning of Pt was present as a uniform effect on all sulfated catalysts, the metal–acid behavior and the different Pt properties could be explained by a metal–support interaction between tetragonal SO_4^{2-}-ZrO_2 and Pt. The Pt–support interaction was analyzed both with a model of Pt particles encapsulation and a model of electron depletion. The electronic deficiency of Pt particles supported on SO_4^{2-}-ZrO_2 was evident in the shift of the IR bands of adsorbed CO. Further experimental work is however needed to get conclusive evidence about the nature of the Pt–support interaction.

Keywords: SO_4^{2-}-ZrO_2; Platinum; Metal–support interaction; *n*-Butane isomerization; *n*-Octane hydroisomerization-cracking; Metal function; Acid function

1. Introduction

It has been reported in several papers that the presence of a noble metal (Pt) greatly enhances the catalytic performance of SO_4^{2-}-ZrO_2 catalysts (SZ) during the hydro conversion of *n*-alkanes [1,2], which are commonly carried out in the presence of H_2 to decrease the coking rate. In these conditions, both the conversion and the selectivity increase and the otherwise easily deactivated catalyst gets stability at a moderate H_2/hydrocarbon ratio [3,4]. Pt/SO_4^{2-}-ZrO_2 catalysts (Pt/SZ) have made their road into the refining industry in the isomerization market niche [5–7]and research continues at industrial labs, trying to get improved catalyst formulations based on the family of oxoanion promoted oxides. As it happens sometimes in the process industry, catalysts have been used while still lacking adequate models of the underlying phenomena related to the catalytic activity. The nature of the active sites of SO_4^{2-}-ZrO_2 and WO_3-ZrO_2 acting in the isomerization step, i.e. on the "acid" site, is still a matter of debate. An even more intriguing point is that of the state of Pt in Pt/SO_4^{2-}-ZrO_2 and Pt/WO_3-ZrO_2. Pt supported on these materials has a negligible chemisorption capacity for

* Corresponding author. Tel.: +54-342-4555279; fax: +54-342-4531068.
E-mail address: cvera@fiqus.unl.edu.ar (C.R. Vera).

0926-860X/$ – see front matter © 2004 Elsevier B.V. All rights reserved.
doi:10.1016/j.apcata.2004.01.010

probe gases (H_2, CO) and other metal properties like hydrogenation of C_6 hydrocarbons are suppressed [8–10].

Though a crystal phase dependence of the catalytic activity of sulfate-zirconia (SZ) catalysts in acid demanding reactions, like *n*-butane isomerization, has previously been reported [11–13], practically no studies have been published on the Pt/SZ counterpart. An assessment of the influence of the crystalline structure of SZ on the properties of the supported metal (Pt) in Pt/SZ catalysts was performed in this work. Pt containing SZ catalysts with different zirconia crystal phases were synthesized: fully tetragonal (T), fully monoclinic (M), and with a mixture of the previous (T + M). Their catalytic properties were studied in the metal-catalyzed reaction of cyclohexane dehydrogenation, the acid-catalyzed isomerization of *n*-butane, and the bifunctional hydroisomerization-cracking of *n*-octane. The results found are discussed in terms of the currently available models that intend to explain the anomalous state of Pt.

The activity of the Pt/SO_4^{2-}-ZrO_2 catalysts for conversion of *n*-octane, one case of bifunctional isomerization-cracking of long chain linear alkanes, is specially studied. Environmental restrictions have lately put a stress on refiners for replacing high octane aromatics and MTBE of the gasoline pool by other additives of similar high octane number. C_8–C_{20} linear paraffins comprise a feedstock that can be valorized by means of its conversion to a mixture of shorter, branched, high RON alkanes that can be blended in the gasoline pool. These branched alkanes not only add RON points but also pose no environmental concern. In the early eighties, Weitkamp [14,15] was one of the first to study the isomerization and hydrocracking of C_6–C_{15} normal alkanes. After further research [16–19], it was clear that a suitable catalyst had to provide both a good isomerizing activity and a mild cracking activity. Due to their good selectivity to isomers at relatively low temperatures, oxoanion promoted zirconia catalysts, WO_3-ZrO_2 or SO_4^{2-}-ZrO_2, have lately concentrated the attention in this field of research. Encouraging results have been reported for isomerization-cracking of medium-length model paraffins and long (C_{16}) paraffins [20–22]. An assessment of the crystal-phase dependence of the activity for this reaction is done in this work.

2. Experimental

2.1. Preparation of unsulfated supports

$Zr(OH)_4$ (ZOH) was obtained by hydrolysis and precipitation of zirconium oxychloride (Strem, 99.99%) with aqueous ammonia. The precipitate was rinsed with distilled water and oven dried at 110 °C overnight. Fully monoclinic zirconia (Z^M) was synthesized with the method of Stichert and Schüth [23]. A zirconia gel was precipitated at a fairly acidic pH (5.6–6.4) and refluxed in its mother liquor for 20 h at 150 °C. The gel was first vacuum dried and then calcined at 400 °C in flowing air (10 ml min^{-1} g^{-1}) to obtain monoclinic zirconia samples. Zirconia with expected mixed crystal phase (M + T) was obtained by calcining ZOH at 620 °C in air for 3 h (Z^{MT} sample). Fully tetragonal zirconia samples were obtained from two sources. Z^TSi was obtained by calcining a silica doped zirconium hydroxide gel (ZOHSi sample, MEL Chemicals, 3.5% fine silica doped) at 620 °C for 3 h in flowing air (10 ml min^{-1} g^{-1}). In order to check the possible interference of the Si dopant, another sample (Z^T) was prepared by following the same synthesis method of the Z^M sample, but changing the pH of precipitation and refluxing to slightly basic pH values (~8.0).

2.2. Preparation of sulfated catalysts

The crystalline samples Z^M, Z^T, Z^TSi and Z^{MT} were impregnated with H_2SO_4 (incipient wetness, Fluka, 2.0N solution). The sulfate content was stabilized by calcination in air (10 ml min^{-1} g^{-1}) at 620 °C for 2 h. The thus obtained catalysts were named S-Z^M, S-Z^T, S-Z^TSi and S-Z^{MT}. The sign (-) is used to indicate that sulfation was performed over crystalline materials, and to make a difference with other ones sulfated in the amorphous state.

As it will be found out later in the Section 3, the catalysts with a mixed phase prepared from crystalline zirconia (S-Z^{MT}) were not very suitable for correlating intermediate levels of catalytic activity with crystal phase content. To sidestep this problem, catalysts with a mixture of phases of varying T/M ratio and with a meaningful level of catalytic activity were obtained by sulfating ZOH samples with different H_2SO_4 solutions of varying concentration, [H_2SO_4], and by using different temperatures of calcination, T_c. The SZ catalysts were thus synthesized. SZ^A: [H_2SO_4] = 0.5N, T_c = 620 °C; SZ^B: [H_2SO_4] = 0.1N, T_c = 620 °C; SZ^C: [H_2SO_4] = 2.0 N, T_c = 620 °C; and SZ^D: [H_2SO_4] = 2.0 N, T_c = 620 °C.

2.3. Pt catalysts

Pt was incorporated to some of the previous samples by incipient wetness impregnation with chloroplatinic acid ($H_2Cl_6Pt{\cdot}6H_2O$, Strem Chem., Pt = 37.5%). The concentration and volume of the solution were adjusted in order to obtain 1% Pt in the final solid. The samples were then oven dried at 110 °C overnight and calcined under flowing air at 500 °C for 2 h. The Pt-loaded catalysts have the prefix "Pt" before the name of the support, e.g. PtZ^M, PtS-Z^{MT}, etc.

2.4. Characterization

Sulfur contents were measured in a LECO CS 444 Carbon Sulfur Analyzer using direct combustion/infrared detection. Hydrogen adsorption isotherms were taken in order to measure the accessibility of the metal phase (Pt). First, samples were heated at 300 °C, reduced in H_2 for 1 h and degassed for 2 h. After cooling to room temperature, isotherms of total and reversible hydrogen adsorption were obtained.

The amount of chemisorbed hydrogen was obtained by subtracting the two isotherms and the H/Pt ratio was calculated assuming dissociative adsorption of hydrogen on the Pt atoms. For the specific surface area, the catalyst samples were degassed at 200 °C for 2 h, and then nitrogen adsorption isotherms were taken at the temperature of liquid nitrogen. A Micromeritics 2100E equipment was used for both measurements.

In order to obtain specimens suitable for transmission electron microscopy studies, the particles were dispersed on a copper grid covered by a carbon film. The samples were observed in a Philips CM200 electron microscope operating at 200 kV, with a point resolution of 0.19 nm. XRD measurements were performed in a Shimadzu XD-1 diffractometer with Cu Kα radiation filtered with Ni. Spectra were recorded in the 20–65° 2Θ range and the scanning rate was 1.2° min^{-1}. The presence of tetragonal (T) and monoclinic (M) phases were distinguished from the reflections at 30.5 and 28°, respectively. The percentage of T and M phase was calculated with the procedure of Mercera et al. [24].

TPR tests were performed in an Ohkura TP2002 equipped with a thermal conductivity detector. The samples were pretreated in situ by heating in Ar at 200 °C for 1 h before each test. Then, they were heated from room temperature to 800 °C at 10 °C min^{-1} in a gas stream of 4.8% H_2 in Ar.

FTIR spectra of pre-reduced, degassed samples were taken at room temperature in a Nicolet 5ZDX spectrometer, in the range 4800–400 cm^{-1} and with a resolution of 4 cm^{-1}. Self supported wafers were successively reduced in flowing hydrogen for (300 °C, 1 h) and outgassed at 10^{-6} Torr at 500 °C for 1 h. After recording the IR spectra, the samples were cooled down to room temperature and contacted with 30 Torr of CO for 10 min and then a new spectrum was recorded. The absorbance of chemisorbed CO was obtained by subtracting the blank from the spectrum of the CO treated sample.

2.5. Catalytic tests

n-Butane isomerization was carried out in a fixed bed quartz reactor operated under isothermal conditions (300 °C) and atmospheric pressure. Reaction products were analyzed by on-line chromatography using a stainless steel column (1/8 in. o.d., 2 m) packed with 25% dimethylsulfolane on Chromosorb P. *n*-C_4 (99.99%) was supplied by AGA. The reaction was performed in pulse mode due to the conditions of very fast deactivation (pulse = 0.2 ml, 6 pulses h^{-1}, carrier = 10 ml N_2 min^{-1}, catalyst mass = 0.3 g) [25].

Cyclohexane (Merck 99.9%) dehydrogenation was performed at 300 °C, 0.1 MPa, catalyst mass = 0.1 g, WHSV = 10 h^{-1} and H_2/C_6H_{12} = 30 (molar ratio). The reaction products were analyzed by on-line chromatography using a packed column (1/8 in. o.d., 2 m) with FFAP on Chromosorb P.

In the hydroconversion of *n*-octane (Carlo Erba RPA), 0.5 g of catalyst ground to 35–80 mesh were used in each reaction test. A tubular reactor was used [17]and reaction conditions were 300 °C, 1.5 MPa, WHSV = 4 h^{-1}, molar ratio H_2/n-C_8 = 6. Maximum time-on-stream was 6 h. From chromatographic data, *n*-C_8 conversion and yields to the different products (on a carbon basis) were calculated.

3. Results

3.1. XRD, sorptometry, S content

Specific surface area and crystal structure data are included in Table 1. The measured XRD spectra confirmed the phase structure supposed for the crystalline sulfate-free zirconias (Z^M, Z^T, Z^TSi and Z^{MT}). ZOH and ZOHSi, were completely amorphous. No peak related to tetragonal zirconia was found on Z^M, which was completely monoclinic, and no peak related to monoclinic zirconia was found on Z^TSi and Z^T, which were completely tetragonal. Zirconia Z^{MT} was mainly monoclinic and had only a small percentage of the T phase. Sulfated samples synthesized from crystalline materials kept the original crystal phase. S-Z^M was fully monoclinic, S-Z^T and S-Z^TSi were fully tetragonal. S-Z^{MT} was mainly monoclinic with a small fraction of T phase.

Most SZ samples contained a mixture of the tetragonal and monoclinic phases, like S-Z^{MT}. The proportion of each phase depended on the synthesis conditions (Table 1, Fig. 1). A dominance of the T phase at higher concentration of the sulfuric acid impregnating solution was found: $SZ^C > SZ^B > SZ^A$. It has been previously reported that the content of T phase in sulfate doped zirconia gels fired at 600 °C

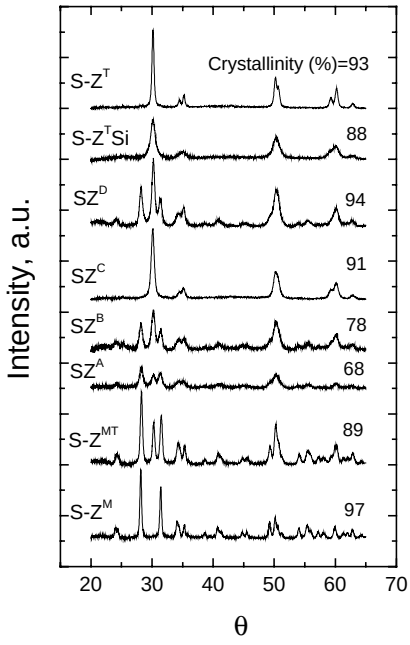

Fig. 1. XRD spectra. Percentage of crystallinity.

Table 1
Textural properties of the samples

Sample	[H_2SO_4] (mol l^{-1}); T_c (°C)[a]	BET area ($m^2\,g^{-1}$)	Sulfur (wt.%)	Crystal phase (vol.%)[b]
Hydroxide				
ZOH	–; 110	262.0	–	Amorphous
ZOHSi	–; 110	275.0	–	Amorphous
Crystalline				
Z^M	–; 400	52.0	–	M(100%)
Z^{MT}	–; 620	37.0	–	M(82%), T(18%)
Z^T	–; 400	59.5	–	T(100%)
Z^TSi	–; 620	68.0	–	T(100%)
Sulfated crystalline				
S-Z^M	2; 620	50.0	0.45	M (100%)
S-Z^T	2; 620	56.4	0.50	T (100%)
S-Z^{MT}	2; 620	33.0	0.38	M (77%), T (23%)
S-Z^TSi	2; 620	63.0	0.69	T (100%)
Sulfated amorphous				
SZSi	2; 620	121.0	1.70	T (100%)
SZ^A	0.5; 620	47.0	0.55	M (78%), T (22%)
SZ^B	1; 620	53.0	0.83	M (62%), T (38%)
SZ^C	2; 620	110.0	1.51	T (100%)
SZ^D	2; 750	71.0	1.02	M (56%), T (44%)

[a] [H_2SO_4]: concentration of the sulfating solution; T_c: calcination temperature.
[b] T: tetragonal; M: monoclinic.

increases with the amount of sulfate added to the hydroxide gel [26]. SZ^C (sulfate doped) was fully tetragonal but it had a lower crystallinity than Z^TSi (96% crystalline, silica doped), indicating that sulfate is a more effective retardant of crystal growth than silica. SZ^D, calcined at 750 °C, had a considerable amount of monoclinic. The tetragonal-to-monoclinic transition is accompanied with sintering and surface area decrease, and in the case of SO_4^{2-}-ZrO_2 catalysts it is associated to the loss of sulfate at temperatures higher than 700 °C. Loss of the stabilizing ion enables the transition from metastable tetragonal to thermodynamically stable monoclinic zirconia [27,28]. Sintering during this transition is a reason why the surface area of SZ^D was lower than that of SZ^C. The area of SZ^D is still higher than SZ^A or SZ^B, but this is a consequence of the lower concentration of H_2SO_4 used in the impregnation of the latter. ZOHSi after sulfation and calcination (SZSi) had a higher surface area and a lower crystallinity than SZ^C. This is the result of the combined effect of silica and sulfate in retarding the sintering and crystallization phenomena. Of the two dopants, silica and sulfate, the latter had the highest stabilization effect when impregnated from a 2N solution, as it can be seen from the comparison of the surface areas: $Z^TSi < SZ^C$,$Z^TSi < SZ^D$.

If we consider that all the sulfur is present on the surface, the calculation of the sulfur surface density after calcination at 600 °C indicates that all samples had a surface density of $\delta = 1.6$–$2.9\,S/nm^2$. On average, this is about half a theoretical monolayer ($\delta = 2\,S/nm^2$), in accord with previously reported values for sulfated zirconia materials with different contents of the T phase [29].

3.2. H_2 chemisorption

The chemisorption of hydrogen on Pt (see Table 2) varied markedly depending on the presence of sulfate. Unsulfated materials had the highest adsorption capacity (H/Pt = 0.16–0.25) while sulfated materials had much lower values (H/Pt = 0.0–0.049). The lowest value was displayed by PtS-Z^T, PtS-Z^TSi and $PtSZ^C$ (H/Pt = 0.0005–0.001). Among the sulfated materials $PtSZ^D$ and PtS-Z^M had the highest adsorption capacities (H/Pt = 0.04–0.049).

In the case of the unsulfated materials, PtZ^M displayed the highest accessibility of Pt by hydrogen (H/Pt = 0.25), while the zirconia samples containing the tetragonal phase had a lower value (0.16–0.23 H/Pt). The capacity for hydrogen chemisorption of these crystalline samples was reduced by sulfate addition but in a different degree in each case. In the case of the mainly monoclinic samples, SZ^M and SZ^{MT}, the reduction was 82–83%. For the other fully tetragonal materials, SZ^T and SZ^TSi, the reduction was much more drastic, 99.4%.

3.3. Transmission electron microscopy

Several micrographs were taken of the $PtSZ^A$, $PtSZ^B$, $PtSZ^C$, $PtSZ^D$ and $PtSZ^T$ catalysts. The size of the Pt particles was measured manually from the micrographs until data sets of 300–500 particles were collected. The main statistical parameters of the distributions are included in Table 1. The dispersion was poor and about 8–10% for the catalysts of the PtSZ series (A–D). These catalysts had Pt particles with an average diameter of 10–12 nm and with a relatively

Table 2
Hydrogen chemisorption (room temperature)

Sample	100 H/Pt	TEM			CH dehydrogenation	
		D[a] (%)	d_m[b] (nm)	σ[c] (nm)	Benzene yield (%)	TON[d] (mol Bz Pt^{-1})
PtZ^M	25.1	–	–	–	35.7	0.091
PtZ^{MT}	17.8	–	–	–	37.5	0.135
PtZ^T	23.0	–	–	–	41.6	0.115
PtZ^TSi	16.1	–	–	–	53.8	0.214
PtS-Z^M	4.4	–	–	–	15.1	0.22
PtS-Z^{MT}	3.0	–	–	–	15.1	0.22
PtS-Z^T	0.15	4.5	20.90	22.04	14.4	6.14
PtS-Z^TSi	0.1	–	–	–	7.7	4.93
$PtSZ^A$	2.0	9.7	9.66	10.01	16.4	0.525
$PtSZ^B$	1.7	9.3	10.11	9.23	7.3	0.275
$PtSZ^C$	0.05	7.6	12.35	12.92	2.4	3.08
$PtSZ^D$	4.9	8.0	11.72	13.44	30.3	0.40

TEM results. Cyclohexane conversion to benzene (300 °C, 1 atm) over the Pt-loaded samples (activity at 1 h time-on-stream).
[a] Dispersion as calculated with TEM data and assuming cubic geometry. $D = 5\rho_S V_a/d_m$, $\rho_S = 12.5$ Pt atoms nm^{-2}, $V_a = 0.0151\,nm^3$ Pt per atom, $D = 0.94/d_m$.
[b] Mean diameter, $\sum f_i d_i$, $i = 1, \ldots, N$ (N: total number of particles).
[c] Standard deviation of the distribution, $\sigma = ((\sum(d_m - d_i)^2)/(N-1))^{0.5}$, $i = 1, \ldots, N$.
[d] Activity per unit of "accessible" Pt atom. Accessibility is that measured by H_2 chemisorption.

wide size distribution (σ, 10–13 nm). $PtSZ^T$ had the lowest dispersion, about 5%, and the widest distribution (σ = 22 nm).The poor dispersion must be related to the Pt impregnation method used. The Pt precursor was a $[PtCl_6]^{2-}$ anion which is electrostatically repelled from the surface of sulfate-zirconia which has a zero-point-of-charge (ZPC) at pH 2 and develops a high negative surface charge at higher pH values [30], like those present in dilute chloroplatinic acid solutions. During the evaporation of the solvent, Pt species might nucleate or oligomerize between themselves due to the temperature and the low affinity for the surface.

3.4. Cyclohexane dehydrogenation

In most cases, benzene was the only compound formed (selectivity 100%) but in some cases some minor amounts of methyl cyclopentane (<5% selectivity) coming from the ring contraction of cyclohexane on the acid function also appeared. Only, the conversion values related to the formation of benzene on the metal function are included in Table 2. As in the case of the results of hydrogen chemisorption, a big difference between sulfated and unsulfated materials can be seen. The conversion of cyclohexane to benzene on unsulfated samples was 36–54% regardless of the structure of the support, indicating that the Pt metal function was working properly and there were no important deactivating factors present. PtZ^TSi had the highest activity in spite of having the lowest dispersion and this could be a beneficial effect of the Si dopant.

In the case of the sulfated samples, the activity in cyclohexane dehydrogenation was smaller, less than one-half that of the unsulfated samples. There seems to be a trend of declining dehydrogenating capacity with the increase of percentage of T structure, i.e. the order of activity is: S-Z^M > S-Z^{MT} > S-Z^T and SZ^A > SZ^B > SZ^C. In the case of the SZ^D sample, the dehydrogenating capacity is one of the highest ones. This result might be the consequence of both the loss of sulfate and conversion to the monoclinic phase. The sulfur content of SZ^D is lower than that of SZ^C because a high amount of sulfate was decomposed at 750 °C. No XPS data was available to see how much of the sulfate lost came from the surface or the bulk. We suppose that an important amount was surface sulfate because SZ^D had an important increase in the volume content of the monoclinic phase. Srinivasan et al. [31] have postulated that the presence of sulfate bridges over surface oxygen vacancies are the cause of the stabilization of the metastable tetragonal phase of zirconia and that the loss of this surface sulfate triggers the tetragonal-to-monoclinic transition.

When we compare the TON values, we can see that there are three groups fairly well defined. Those catalysts with normal H accessibility (100 H/Pt > 10), i.e. the catalysts without sulfate, have TON values of 0.09–0.21 mol Pt^{-1}. The catalysts with low H accessibility (1 < 100 H/*Pt* < 10), i.e. mixed phase (T + M) sulfated catalysts $PtSZ^A$, $PtSZ^B$, $PtSZ^D$ and $PtSZ^{MT}$, and monoclinic Pt-SZ^M, have TON values of 0.22–0.6 mol Pt^{-1}. Finally, those catalysts with very low H accessibility (100 H/Pt < 1), i.e. the sulfated fully tetragonal PtS-Z^T, PtS-Z^TSi and $PtSZ^C$, have TON values of 3–6 mol Pt^{-1}. This high value of TON is difficult to explain and must be related to an abnormal state of Pt when supported on SO_4^{2-}-ZrO_2. Vannice [32] has pointed out that TON values of metal-catalyzed reactions occurring on metal particles suffering from strong metal–support interaction should be handled with care. Most likely cyclohexane dehydrogenation is performed over a higher amount of Pt surface sites than those titrated in the static chemisorption tests. Rajeshwer et al. [33] have noted that H chemisorption

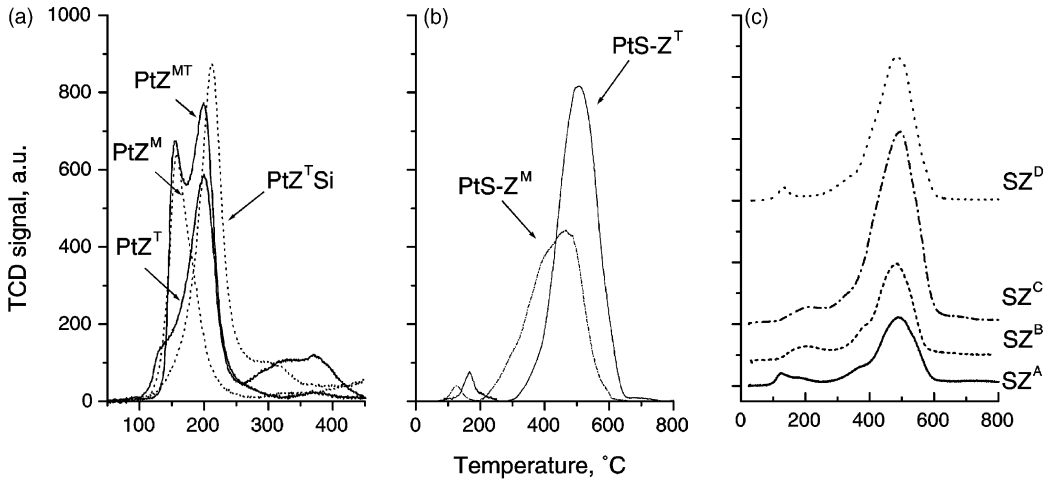

Fig. 2. TPR tests: (a) Pt over unsulfated zirconia (PtZ); (b) Pt over zirconia sulfated in the crystalline state (PtS-Z^M and PtS-Z^T); and (c) Pt over zirconia sulfated in the amorphous state (PtSZ).

is quite a sensitive property and that the reaction becomes activated when Pt ensembles are perturbed. In their case, the presence of Sn atoms diminished the amount of chemisorbed hydrogen. The amount of H chemisorbed augmented when the temperature was raised.

3.5. Temperature-programmed reduction

We have seen that the dehydrogenation capacity of the metal was practically not influenced by the crystal phase in the case of the non-sulfated catalysts and the same happened with the metal accessibility as measured by H chemisorption. Pt reducibility however seemed to be influenced by the crystal phase of the support. The TPR results of sulfur-free catalysts displayed two different and very definite peaks on the samples, one at a low temperature (150–160 °C) and another at a higher temperature (200–220 °C) (Fig. 2a). The presence of two kind of Pt species of different reducibility cannot be attributed to differences in dispersion because the sulfur-free catalysts had no big differences in H/Pt chemisorption values, especially in the case of the PtZ^M and PtZ^T catalysts. For this reason the differences in reducibility could be related to the interaction of the Pt particles with domains of the zirconia support of different crystal and surface properties. The high temperature peak was attributed to the reduction of Pt particles of lower reducibility supported over tetragonal crystallites with a closely packed eight-fold coordination of the Zr lattice. The low temperature peak was attributed to the reduction of Pt particles of higher reducibility which were supported over monoclinic crystallites with Zr surface cations of seven-fold coordination. These assumptions can be readily be confirmed by inspection of the TPR plots of PtZ^M and PtZ^TSi, which have only one crystal type and only one kind of TPR peak present. In the case of PtZ^T and PtZ^{MT}, these catalysts had both types of peaks present, though the low temperature peak in the case of PtZ^T was very small (<5% total area) and was shifted to 130 °C. Pt on Z^{MT} was mainly reduced at 200–220 °C and about 40% was reduced at 150–160 °C. This sample had been shown to be mainly monoclinic by XRD inspection. The bigger size of the high temperature peak, associated to Pt on tetragonal crystals, might pose an apparent discrepancy but could be explained by supposing either a preferential deposition of Pt over Z^T or a greater contribution of tetragonal crystals to the total area due to the presence of small high surface area tetragonal crystallites. It was early reported [34] that the tetragonal phase is stabilized in very small crystallites due to the higher surface energy of monoclinic zirconia.

In the case of the TPR plots of Pt supported over sulfated zirconia (Fig. 2b) while the shift in the peak of Pt reduction to higher temperatures in the case of the tetragonal sample is also present, there is another small shift and a different size of the main peak of sulfate reduction. These differences are due to the smaller area of S-Z^M and the associated smaller sulfur content.

In the case of the TPR plots of Pt supported over sulfated zirconia, Fig. 2c, we can distinguish two main peaks. The small peak at 100–300 °C is seemingly due to the reduction of Pt while the peak at 350–650 °C is due to the reduction of surface sulfate groups.

The plots of Fig. 2c correspond to reduction experiments performed with materials sulfated in the amorphous state with different sulfuric acid concentrations and calcined at different temperatures. The areas of the main peak of sulfate reduction correlate with the sulfur content of the catalysts. The catalysts treated with a higher sulfuric acid concentration have a bigger area, when the temperature of calcination is the same ($SZ^A < SZ^B < SZ^C$). The relative size of the sulfate reduction peak also indicates that the amount of sulfate decreases for a given concentration (2.0N) when the temperature of calcination increases ($SZ^C > SZ^D$).

The zone of Pt reduction for the group of sulfated catalysts is located at 100–250 °C. For $PtSZ^B$ and $PtSZ^C$, the Pt reduction peak is located at about 200 °C while for $PtSZ^A$

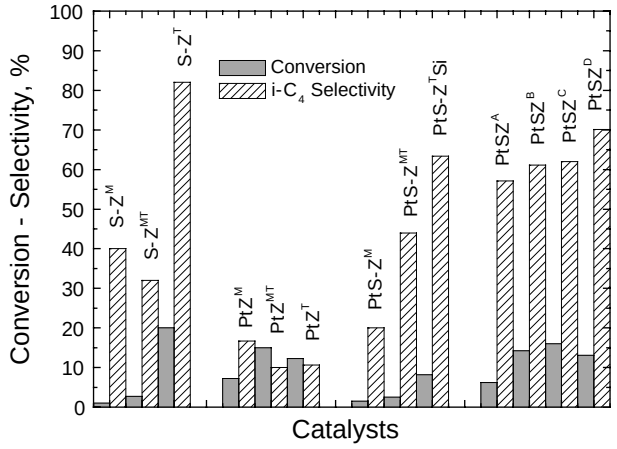

Fig. 3. Isomerization of *n*-butane (pure, undiluted). Average of first 30 pulses.

and $PtSZ^D$ the reduction peak is located at 100–150 °C. We can see that the samples with a high content of T phase show the higher shifts: SZ^C, $SZ^B > SZ^D$, SZ^A.

3.6. n-Butane isomerization

Some samples showed high initial conversion values but their activity dropped sharply after the first pulses. For this reason, it seemed convenient to take an average of the conversion of the first 30 pulses as a measure of the activity level. Results of isobutane yield for all catalysts are included in Fig. 3. In the case of the Pt-free catalysts, activity was maximum for the $S\text{-}Z^T$ sample, with an average conversion of 20% and an average selectivity to $i\text{-}C_4$ of 82% (16% yield). Deactivation was fast and the conversion dropped to about 13% the initial value in the 30th pulse (1st pulse = 68%, 30th pulse = 9%). $S\text{-}Z^M$ had a negligible activity (1% conversion) and a medium selectivity (40%). In the case of $S\text{-}Z^{MT}$, the average conversion was about 3% while the selectivity was only 32%.

The results corresponding to the Pt-loaded catalysts can also be found in Fig. 3. The unsulfated catalysts showed a cracking activity attributed to the metal function and their selectivity to isomers was very low (10–16%), much lower than that of their sulfated counterparts, indicating that sulfate is needed for the presence of a reaction pathway leading to skeletal branching.. Their yield of isobutane was overall low (about 1.3%).

In the case of the catalysts which were sulfated after their calcination (crystalline supports), the activity was maximum for the catalysts with tetragonal structure and the reactivity order was opposite to that found in the case of cyclohexane dehydrogenation: $PtS\text{-}Z^M < PtS\text{-}Z^{MT} < PtS\text{-}Z^T \approx PtS\text{-}Z^TSi$. From left to right, both the selectivity and the conversion increase (conversion: 1.5–8%; selectivity: 20–64%). The catalysts sulfated in the state of amorphous gel (PtSZ series) had both high conversion and selectivity values (12.5 and 62.6% on average), though their activity was lower than that of $S\text{-}Z^T$. Inside the series, the activity increased from A to C and then dropped from C to D. This pattern follows approximately the variations of sulfate concentration on the final catalyst and the ratio (yield of isobutane/sulfur %) varies in a fairly narrow band of 6.4–10.4. This correlation between sulfate content and activity can only be found in this series of catalysts because they all have an important amount of tetragonal active phase.

3.7. Hydroconversion of n-octane

Cyclohexane dehydrogenation is a strictly metal catalyzed reaction and *n*-butane isomerization an acid catalyzed one. Apart from being a reaction of interest in this work, the results of *n*-octane hydroisomerization help in elucidating the contribution of the metal and acid functions because the reaction can proceed by an acid-catalyzed monofunctional pathway or a bifunctional metal–acid catalyzed one [35]. The results of this test are shown in Figs. 4 and 5.

The conversion drops severely in the case of the Pt-free catalysts (Fig. 4a) due to deactivation by coking. This activity drop is specially noticeable in the case of the catalysts with higher activity, SZSi and SZ^C, which lose 80% of their initial activity after 1 h of time-on-stream.

In the case of the Pt-loaded catalysts, conversion was high for the $PtS\text{-}Z^T$, $PtSZ^C$ and PtSZSi fully tetragonal catalysts and it was highest for those impregnated in the amorphous state, $PtSZ^C$ and PtSZSi. Olefin formation on Pt particles must have been very low, as revealed by the test of cyclohexane dehydrogenation, but the amount of olefins formed must have been enough to form a sizable pool that enables the onset of a bifunctional mechanism. The presence of a bifunctional mechanism in the case of the Pt and sulfate-loaded catalysts can be acknowledged on the basis of the great increase in the level of activity with respect to the sulfate-loaded, Pt-free samples. The metal activity, though highly depressed, was also enough for producing activated hydrogen, necessary for hydrogenating coke precursors and keeping a stable conversion level.

The activity was almost negligible for the fully monoclinic samples. In the case of the PtSZ catalysts series, the activity order found was: $PtSZ^A < PtSZ^B < PtSZ^D < PtSZ^C$. For these catalysts, this is also the order of increasing sulfur content and increasing T phase content.

Fig. 5 contains data of total conversion and yield to individual isomers. The most active catalysts, $PtSZ^C$ and PtSZSi, display the minimum yield of isooctane and the maximum yield of isobutane. The conversion level and the selectivity pattern of $PtSZ^D$ and $PtS\text{-}Z^T$ are also similar. Their $i\text{-}C_4$ and $i\text{-}C_8$ yields are almost equal Comparing with $PtSZ^C$ and PtSZSi it can be seen that the decrease in the yield of $i\text{-}C_{4–7}$ is accompanied by an increase in the yield of $i\text{-}C_8$ and vice versa.

The selectivity to isooctane grows with conversion and the opposite occurs with the selectivity to isobutane. The isomer distribution seems to be uniquely a function of conversion, as

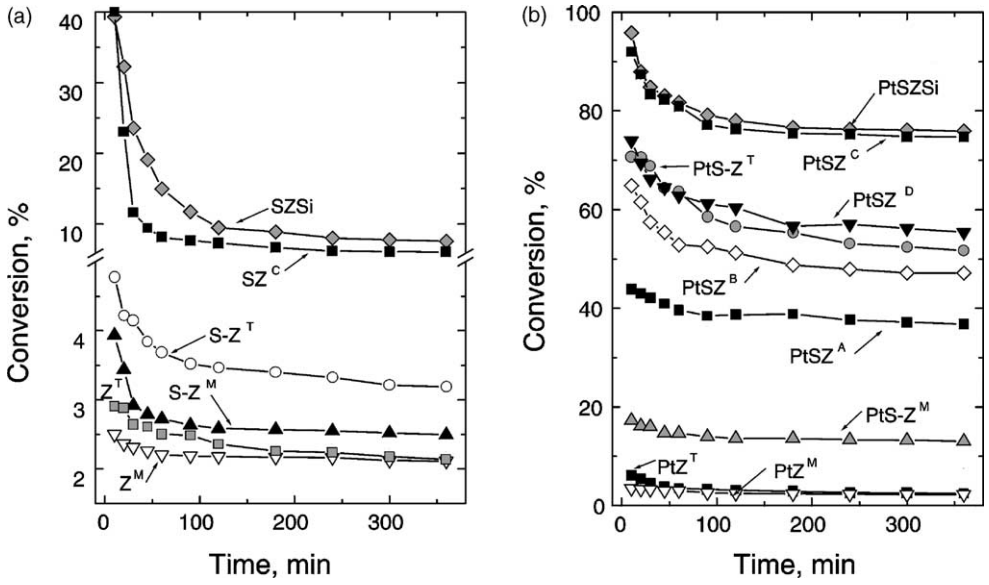

Fig. 4. Activity in hydroisomerization-cracking of *n*-octane: (a) Pt-free catalysts and (b) Pt-containing catalysts.

is often the case for hydroconversion over a series of similar catalysts having sufficient acid and metal functionality.

3.8. FTIR

Spectra of the catalysts after reduction and before CO adsorption in the wave number range between 1200 and 3800 cm^{-1} are shown in Fig. 6. It is known that the modification of ZrO_2 with sulfate ions substantially increases the acidic properties of this oxide [36]. In the case of the ν_{OH} stretching range, 3000–3850 cm^{-1}, vibrations due to tri-coordinated OH (3630–3720 cm^{-1}), di-coordinated OH (3740–3770 cm^{-1}) and mono-coordinated OH (3780–3810 cm^{-1}) have been identified on zirconia [37,38]. All the supports had an important amount of tri-coordinated OH groups. The amount of di-coordinated OH groups was important only in the case of the Z^T and SZ^T samples.

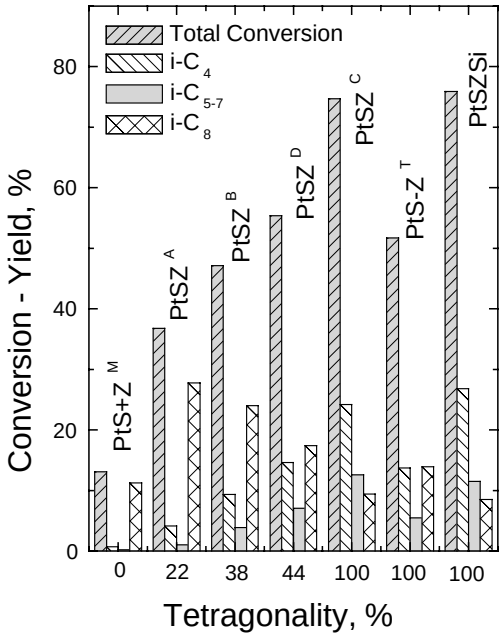

Fig. 5. Total conversion and yield to different products in hydroisomerization-cracking of *n*-octane. Pt-containing catalysts. Time-on-stream = 6 h.

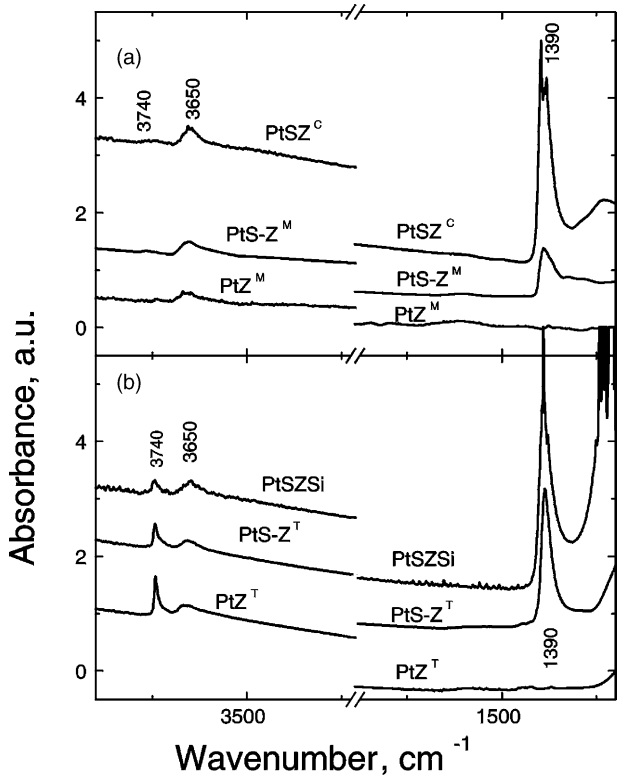

Fig. 6. IR spectra (samples evacuated to a level of 10^{-6} mmHg residual pressure).

Tri-coordinated OH groups were dominant on the zirconia gel sample (ZOH, not shown) and on the monoclinic samples. Upon sulfation and calcination, the amount of OH groups decreases and a new band at 1390 cm^{-1} due to the vibration of covalent sulfate groups on a highly dehydrated surface appears [39,40]. The data of Fig. 6 indicates that the final distribution of OH coordination groups on the sulfated catalysts was different depending on the sample, but in most cases tri-coordinated OH groups prevailed. In the case of the most active catalysts, which were fully tetragonal and had a comparable level of conversion in the *n*-C_4 and *n*-C_8 tests, i.e. the $PtSZ^C$, $PtS\text{-}Z^T$ and PtSZSi samples, the di/tri-coordinated ratio was either practically zero, close to unity or higher than one. This lack of correlation between activity of sulfated-zirconia and abundance of different coordination families of OH groups has been recently stressed [41].

The IR spectra of CO adsorbed on both series of reduced catalysts had three absorption bands in the region of CO stretching vibrations: a high frequency band corresponding to CO complexes with Lewis acid sites (ν_{CO} = 2190–2200 cm^{-1}) [42], a broad band corresponding to linear adsorption of CO on Pt (ν_{CO} = 2070–2094 cm^{-1}) and a low frequency band located at ν_{CO} = 1855 cm^{-1} corresponding to bridge adsorption of CO on Pt [43,44]. When the catalysts are sulfated the area of the this band due to Lewis acid sites is increased and the frequency of the peak is shifted to higher frequency values. At about the same frequency, oxidized samples of PtSZ have an absorption band characteristic of CO complexes with Pt^{2+} ions [43,44]. This band might not be present in our case because our catalysts were previously reduced at 300 °C.

The band with a maximum at ν_{CO} = 2074–2094 cm^{-1} is broad and corresponds to CO linearly adsorbed on Pt. Deconvolution of this broad absorption band allows distinguishing several elemental bands. The elemental band at 2120 cm^{-1} can be assigned to the vibrations of CO adsorbed on $Pt^{\delta+}$, an electron deficient Pt [44]. This band is small on PtZ^M and even smaller on PtZ^T. Upon addition of sulfate this band increases, and to a greater extent on $PtS\text{-}Z^T$ than on $PtS\text{-}Z^M$. The elemental band at 2140–2150 cm^{-1} can be ascribed to Pt^+ [29,43,44], which is present only on the tetragonal materials sulfated in the amorphous state.

The deconvoluted great absorption band at 2070–2094 cm^{-1} can be assigned to CO adsorbed on Pt^0 [36]. Strictly the oxidation state is not zero because there is a shift of the band towards higher frequencies, compared to Pt^0 supported on inert supports. For all catalysts, this Pt^0 band is the largest, which should indicate that a great part of Pt is in the metallic state. This conclusion does not agree with the low hydrogen chemisorption on these materials. The reason must be the electron deficient character of this Pt. An absorption band at 2049–2064 cm^{-1} appears on all the catalysts. This low frequency band was very small in the IR spectra of Ivanov and Kustov [44] and was not considered by these authors. The band produces a tail in the low frequency range and seems to be the envelope of several lower bands. In this sense this band could be the envelope of bands due to linear CO adsorbed on Pt^0 of crystals of smaller size [45].

In the case of the sulfate-free samples, there exists a different position of the CO band at 2070–2094 cm^{-1} when Pt is supported on tetragonal zirconia (PtZ^T) or monoclinic zirconia (PtZ^M). This band is positioned at a higher frequency in the PtZ^M sample. Shifts in the frequency of adsorbed species are expected to be found because of the different nature of the monoclinic (M) and tetragonal (T) surfaces. The effective Mulliken charge (in units of electrons) of bulk O and Zr atoms in T and M zirconia is very similar: Zr = 2.05 and O = 6.97 in zirconia T and Zr = 2.09 and O = 6.95 in zirconia M [46]. However, zirconia M has a higher surface energy (σ_M = 1130 ergs/cm^2, σ_T = 770 ergs/cm^2) than zirconia T [34]. Zirconia T, with a coordination number of 8, is more densely packed than zirconia M, which is seven-fold coordinated, and should have less shielded surface Zr cations. An inspection of the bands at 2191–2196 cm^{-1} of Fig. 7 for

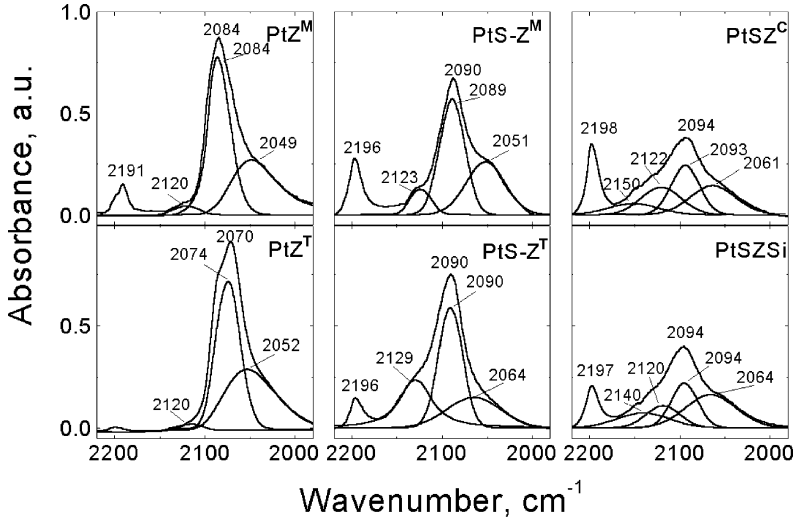

Fig. 7. IR spectra of CO species adsorbed on Pt supported over sulfated and unsulfated zirconia.

Z^T and Z^M shows that the area of the band is almost negligible for PtZ^T and quite significant for PtZ^M, indicating the presence of strong Lewis sites on Z^M. The interaction of zirconia M with Pt particles seems to produce some electron depletion as evidenced by the shift of the CO adsorption peak (2070–2090 cm^{-1}) relative to zirconia T. The effect is smeared upon sulfation of the samples. Sulfation itself produces a bigger shift of the CO/Pt^0 band to 2090–2094 cm^{-1} and increases the size of the CO/(Lewis acid site) bands on both T and M samples to comparable sizes while shifting their position to 2196–2197 cm^{-1}.

The former analysis of the IR spectra indicates a change in the electronic state of Pt. In all cases, there is a shift toward higher frequencies which is assigned to the adsorption of CO over electron deficient Pt. In the case of tetragonal ZrO_2 sulfated in the amorphous state, three forms of Pt (Pt^+, $Pt^{\delta+}$ and Pt^0) can co-exist on the surface of sulfated zirconia, according to the electronic transfer from Pt to the support. It seems that Pt has both heterogeneity in electronic density and in particle size. TEM data indeed indicated that SZ^A, SZ^B, SZ^C, SZ^D and S-Z^T had a broad distribution of particle sizes (σ = 9–22 nm). Most probably, the different bands are a consequence of the size of the particle and its position on the support.

4. Discussion

Recently, we have reported a significant influence of the crystalline structure of ZrO_2 on the metallic properties of Pt, when supported on WO_3-ZrO_2 [47]. Pt supported on tungsten-doped tetragonal zirconia lost its metallic properties while when supported on monoclinic zirconia it had good metal activity. WO_4^{3-} deposited over amorphous $Zr(OH)_4$ generated after calcination an active material for *n*-butane isomerization. The larger the fraction of the tetragonal phase of zirconia in this material, the higher the isomerization activity and the lower the dehydrogenation activity. The results of the present work with SO_4^{2-}-ZrO_2 confirm this general trend.

There is a decrease in metal properties common to all the catalysts which might be attributable to sulfur poisoning. If a comparison is made between the catalysts while trying to subtract this effect, we can see that there still exist differences between the Pt particles supported on M and T samples. In the case of the chemisorption of hydrogen, the adsorption capacity is decreased to 3–5% on the monoclinic and mixed phase catalysts, while on the fully tetragonal catalysts the adsorption drops to less than 0.2%. The benzene yield on these T catalysts (S-Z^T, S-Z^TSi, SZ^C) also decreases with respect to their monoclinic and mixed phase counterparts. The decrease in the yield is however not so sharp and as a result the TON values for the cyclohexane reaction on these catalysts take abnormally high values. Completely different effects are seen in the case of *n*-butane isomerization. The catalysts having the lower yields of benzene, the fully tetragonal ones, now have the higher yields of isobutane. Monoclinic catalysts are inactive and mixed phase catalysts (S-Z^{MT}, SZ^A, SZ^B, SZ^D) have an intermediate activity level. Similar results are found in the case of the *n*-octane reaction. Fully tetragonal catalysts display the highest conversion values and the highest yields of isobutane, while the activity gradually decreases following approximately the order of decreasing tetragonality (Fig. 6): SZ^TSi > SZ^C > SZ^D, S-Z^T > SZ^B > SZ^A > SZ^M. In the case of the CO adsorption experiments, the tetragonal samples sulfated in the amorphous state have Pt particles in the highest electron deficient state, showing bands of Pt^+ and $Pt^{\delta+}$, and intensity-decreased bands of Pt^0. The samples sulfated in the crystalline state lack the band due to Pt^+, while the $Pt^{\delta+}$ band is bigger and of higher frequency on the fully T sample (S-Z^T).

The current results add to the currently accumulated empirical evidence indicating that the combination of the tetragonal phase and the presence of electronegative oxoanions that promote the activity in acid-catalyzed reactions, inhibits the metal activity of supported Pt. It is worth noting that none of the models trying to explain the anomalous state of Pt have taken these facts into account. A revision of these models follows.

The formation of a stable PtO_x phase on the surface of Pt particles has been suggested by some authors [48]. The model tried to reconcile results related to the detection of both oxidized Pt (by TPR, H_2 chemisorption, XPS) and metallic Pt (by XRD). EXAFS results were interpreted as coming from 20% surface cationic Pt (like PtO) and 80% bulk metallic Pt^0.

Sulfur poisoning was the first hypotheses early posed by some authors. Paál and co-workers stated that Pt was sulfided after activation of Pt/SO_4^{2-}-ZrO_2 [49] and Iglesia et al. [50] proposed that Pt was present as a metal sulfide. More recently, Xu and Sachtler [51] have suggested that H_2S formed in the presence of H_2 and Pt poisons the Pt particles.

An electronic effect due to adsorbed species (H^+) has also been posed. Ivanov and Kustov [44] reported shifts in the infrared bands of CO complexes adsorbed on Pt when the metal was deposited on SZ. These shifts were related to the formation of electron deficient $Pt^{\delta+}$ on SZ. Electron depletion was addressed to acidic delocalized protons interacting with the surface of Pt.

The above described models do not take into account explicitly the crystal phase of the support and cannot be modified to include it in an easy way. Other models must be considered if the results obtained in this work are to be rationalized. Paál and co-workers [52,53] suggested that in the case of Pt/SO_4^{2-}-ZrO_2 catalysts the Pt particles are buried in the first layers of the ZrO_2 support. Though formation of ZrO_2 overlayers is hardly reported in the literature [54], the model was supported on results of ion scattering spectra (ISS) of fresh and calcined Pt/SO_4^{2-}-$Zr(OH)_4$. The ISS Pt peak disappeared after calcination. It is however difficult to reconcile our results with the idea of Pt encapsulation. In all

our catalysts, Pt was incorporated over an already crystalline support and therefore migration of suboxide species could only occur during activation of the metal function and during the test (chemisorption, reaction) itself. Encapsulation during crystallization of the gel, as it could be the case with the catalysts of refs. [52,53] is ruled out in our case. Analyzing the data of Table 1, we see that there were practically no differences in Pt accessibility in the group of sulfur-free catalysts irrespective of the phase of the support. Moreover, in order to explain the differences in H chemisorption, it should be accepted that encapsulation occurs preferentially on tetragonal catalysts and in the presence of sulfate. If we finally turn our attention to the IR results, we see that the CO bands of Pt^0 rather than disappearing, are only decreased, and that new bands of cationic Pt appear, results which are difficult to explain on the basis of encapsulation of Pt.

An electronic model could be considered suitable if some dependence on the crystal phase were included in it. The IR results undoubtedly indicate that an electron deficiency of the Pt particles appear when the catalyst is sulfated and that this deficiency is enhanced when the support is tetragonal. In some cases, not only the $Pt^{\delta+}$ band is increased and shifted to higher frequencies (as in PtS-Z^T) but also a band of cationic Pt^+ appears (PtSZ^C, PTS-Z^TSi). IR and H chemisorption results could be explained if we accept that sulfate groups deplete from electrons the surroundings of Pt particles and that electrons in Pt move to the zirconia interface due to an induction effect, leaving some particles in a polarized state and others in a cationic state. This electronic effect would be enhanced on tetragonal zirconia and a possible explanation follows.

We have recently proposed [41] that anionic vacancies ($VO^{\bullet}$, $VO^{\bullet\bullet}$) in active SO_4^{2-}-$Zr(OH)_4$ catalysts produce the stabilization of the tetragonal phase by lowering the average coordination number of Zr, and also contribute to the appearance of *n*-type conductivity by narrowing the band gap of the oxide. Such defects would be absent in monoclinic catalysts. It is also known that *n*-type oxides can produce surface electronic interactions through their conduction band. In this sense, electron depletion by electronegative sulfate (or tungstate) groups it is expected to occur through the Pt–support interface of non-stoichiometric (tetragonal) zirconia. Though this model of electron depletion can accommodate the experimental results it is difficult to verify without the completion of specialized tests.

5. Conclusions

The anomalous state of Pt in Pt/SO_4^{2-}-ZrO_2 catalysts (negligible chemisorption of H_2, poor dehydrogenating properties, shift in TPR peak, positively charged by IR) while being always present when the zirconia support is sulfated, it is enhanced when the crystal phase of the catalyst is tetragonal. In the absence of sulfate, the interaction between Pt and the support is much lower and practically no abnormal properties are detected.

Monoclinic Pt/SO_4^{2-}-ZrO_2 catalysts, had low activity in *n*-butane isomerization and had high activity in cyclohexane dehydrogenation. Tetragonal catalysts were the most active in *n*-butane isomerization and had the lowest activity in cyclohexane dehydrogenation. Mixed phase catalysts had an intermediate behavior. The low metal activity of Pt is enough in the case of the reaction of *n*-octane hydroisomerization, and a bifunctional mechanism with a good level of conversion and stability is found.

While strong sulfur poisoning of Pt seems undoubtedly present in the sulfated zirconia catalysts, the results related to the varying metal properties are better explained if a strong, crystal phase dependant, metal–support interaction is supposed to be present. This interaction, which would be especially strong in tetragonal Pt/SO_4^{2-}-ZrO_2 catalysts was tried to be rationalized both with a model of encapsulation of Pt particles and with a model of depletion of electrons from the zirconia interphase. The electrodeficiency of Pt detected in the IR experiments and the differences in chemisorption found in our catalysts are difficult to explain with the first model. In the case of the second model, electron withdrawal from the zirconia interphase would be enhanced in tetragonal zirconia due to the induction of electronegative sulfate through the conduction band of the support. This model seems to explain the results better but an adequate assessment of charge transfer phenomena in the bulk and surface of sulfated zirconia is still lacking.

References

[1] T. Hosoi, T. Shimidzu, S. Itoh, S. Baba, H. Takaoka, T. Imai, N. Yokoyama, N., in: Proceedings of the American Chemical Society, Los Angeles, 1988, p. 562.
[2] K. Ebitani, J. Konishi, A. Horie, H. Hattori, K. Tanabe, in: K. Tanabe, H. Hattori, T. Yamaguchi, T. Tanaka (Eds.), Acid–Base Catalysis, Kodansha, Tokyo, 1989, p. 491.
[3] J.C. Yori, M.A. D'Amato, G. Costa, J.M. Parera, J. Catal. 153 (1995) 218.
[4] R.A. Comelli, S.A. Canavese, S.R. Vaudagna, N.S. Fígoli, Appl. Catal. 135 (1996) 287.
[5] Ch.D. Gosling, R. Rosin, P. Bullen, T. Shimizu, T. Imai, Pet. Technol. Q. (1997/1998) 55.
[6] P.G. Blommel, Ch.D. Gosling, S.A. Wilcher, US Patent 5,763,713 (1998).
[7] Ch.D. Gosling, P.G. Blommel, M.J. Cohn, R.D. Gillespie, J.S. Holmgren, US Patent 5,837,641 (1998).
[8] K. Ebitani, H. Konno, T. Tanaka, H. Hattori, J. Catal. 143 (1993) 322.
[9] T. Shishido, T. Tanaka, H. Hattori, J. Catal. 172 (1997) 24.
[10] K. Ebitani, J. Tsuji, H. Hattori, H. Kita, J. Catal. 135 (1992) 609.
[11] R.A. Keogh, B.H. Davis, Catal. Lett. 57 (1999) 242.
[12] C.R. Vera, J.C. Yori, C.L. Pieck, J.M. Parera, Appl. Catal. 240 (2003) 161.
[13] W. Stichert, F. Schüth, S. Kuba, H. Knözinger, J. Catal. 198 (2001) 277.
[14] J. Weitkamp, Ind. Eng. Chem. Prod. Res. Dev. 21 (1982) 550.
[15] J. Weitkamp, P.A. Jacobs, J.A. Martens, Appl. Catal. 8 (1983) 123.

[16] J.A. Martens, R. Parton, L. Uytterhoeven, P.A. Jacobs, G.F. Froment, Appl. Catal. 76 (1991) 95.
[17] J.M. Grau, J.M. Parera, Appl. Catal. 106 (1993) 27.
[18] F. Alvarez, F.R. Ribeiro, G. Perot, C. Thomazeau, M. Guisnet, J. Catal. 162 (1996) 179.
[19] J.A. Muñoz Arroyo, G.G. Martens, G.F. Froment, G.B. Marin, P.A. Jacobs, J.A. Martens, Appl. Catal. A 192 (2000) 9.
[20] J.M. Grau, J.M. Parera, Appl. Catal. A 162 (1997) 17.
[21] S. Zhang, Y. Zhang, J.W. Tierney, I. Wender, Appl. Catal. 193 (2000) 155.
[22] R.A. Keogh, B.H. Davis, Catal. Lett. 57 (1999) 33.
[23] W. Stichert, F. Schüth, J. Catal. 174 (242) (1998) 242.
[24] P.D.L. Mercera, J.G. van Ommen, E.B.M. Doesburg, A.J. Burggraaf, J.R.H. Ross, Appl. Catal. 57 (1990) 127.
[25] C.R. Vera, C.L. Pieck, K. Shimizu, C.A. Querini, J.M. Parera, J. Catal. 187 (1999) 39.
[26] F.-Ch. Wu, Sh.-Ch. Yu, J. Cryst. Growth 96 (1989) 96.
[27] F.G.R. Gimblett, A. Hussain, K.S.W. Sing, J. Therm. Anal. 34 (1988) 1001.
[28] F.R. Chen, G. Coudurier, J.-F. Joly, J.C. Vedrine, J. Catal. 143 (1993) 616.
[29] C. Morterra, G. Cerrato, S. Di Ciero, M. Signoretto, F. Pinna, G. Strukul, J. Catal. 165 (1997) 72.
[30] J.M. Grau, C.R. Vera, J.M. Parera, Appl. Catal. 172 (1998) 311.
[31] R. Srinivasan, T.R. Watkins, C.R. Hubbard, B.H. Davis, Chemistry of Materials 7 (1995) 725.
[32] M.A. Vannice, in: Proceedings of the 214th ACS National Meeting, Las Vegas, NV, 7–11 September 1997, p. 861.
[33] D. Rajeshwer, A.G. Basrur, D.T. Gokak, K.R. Krishnamurthy, J. Catal. 150 (1994) 135.
[34] R.C. Garvie, J. Phys. Chem. 69 (1965) 1238.
[35] J.M. Grau, J.C. Yori, J.M. Parera, Appl. Catal. 213 (2001) 247.
[36] L.M. Kustov, V.B. Kazansky, F. Figueras, D. Tichit, J. Catal. 150 (1994) 143.
[37] T. Yamaguchi, Y. Nakano, K. Tanabe, Bull. Chem. Soc. Jpn. 51 (1978) 2482.
[38] G. Cerrato, S. Bordiga, S. Barbera, C. Morterra, Appl. Surf. Sci. 115 (1997) 53.
[39] T. Jin, T. Yamaguchi, K. Tanabe, J. Phys. Chem. 90 (1986) 4794.
[40] M. Bensitel, O. Saur, J.-C. Lavalley, B.A. Morrow, Mater. Chem. Phys. 19 (1988) 147.
[41] C.R. Vera, C.L. Pieck, K. Shimizu, J.M. Parera, Appl. Catal. 230 (2002) 137.
[42] C. Morterra, R. Aschieri, M. Volante, Mater. Chem. Phys. 20 (1988) 539.
[43] A.V. Ivanov, L.M. Kustov, T.V. Vasina, V.B. Kazanskii, P. Zeuthen, Kinet. Katal. 38 (1997) 403.
[44] A.V. Ivanov, L.M. Kustov, Russ. Chem. Bull. 48 (1999) 1061.
[45] M.J. Kappers, J.T. Miller, D.C. Koningsberger, J. Phys. Chem. 100 (1996) 3227.
[46] F. Zandiehnadem, R.A. Murray, Y. Ching, Physics B 150 (1988) 19.
[47] J.C. Yori, J.M. Parera, Catal. Lett. 65 (2000) 205.
[48] T. Shishido, T. Tanaka, H. Hattori, J. Catal. 172 (1997) 24.
[49] Z. Paál, M. Muhler, R. Schrol, J. Catal. 143 (1993) 318.
[50] E. Iglesia, S.L. Soled, G.M. Kramer, J. Catal. 144 (1993) 238.
[51] B.-Q. Xu, W.M.H. Sachtler, J. Catal. 167 (1997) 224.
[52] Z. Paál, U. Wild, M. Muhler, J.-M. Manoli, C. Potvin, T. Buchholz, S. Sprenger, G. Resofszki, Appl. Catal. 188 (1999) 257.
[53] J.-M. Manoli, C. Potvin, M. Muhler, U. Wild, G. Resofszki, T. Buchholz, Z. Paál, J. Catal. 178 (1998) 338.
[54] K. Asakura, Y. Iwasawa, S.K. Purnell, B.A. Watson, M.A. Barteau, B.C. Gates, Catal. Lett. 15 (1992) 317.